Available online at www.sciencedirect.com
SCIENCE DIRECT®
PERGAMON
International Journal of Heat and Mass Transfer 46 (2003) 4553–4559
International Journal of HEAT and MASS TRANSFER
www.elsevier.com/locate/ijhmt

Technical Note

2D-heat transfer modelling within limited regions using moving sources: application to electron beam welding

D. Couëdel [a], P. Rogeon [a,*], P. Lemasson [a], M. Carin [a], J.C. Parpillon [b,1], R. Berthet [b,1]

[a] *LET2E: Laboratoire d'Etudes Thermique Energétique et Environnement, U.B.S, Centre Universitaire de Recherche, rue Saint Maudé 56325 Lorient Cedex, France*
[b] *DCN Indret: 44620 La Montagne, France*

Received 10 January 2002; received in revised form 5 May 2003

Abstract

2D or 3D analytical models currently available in the literature are usually restricted to infinite regions. An original 2D-analytical model to calculate thermal cycles in regions of limited width using a vibrated/non-vibrated moving thermal source, has been developed here. First, the impact of the source size and then, the influence of the boundary on the thermal field within the limited region has been discussed. Finally, the model has been applied to electron beam welding and validated, concerning thermal kinetics, by comparison with experimental thermal cycles.

1. Introduction

A good knowledge of the temperature field given by a moving source within a material is obviously of the greatest practical interest for the study of welding processes (Electron beam welding, Laser beam welding, arc welding). Many analytical 2D- or 3D-models have been developed in the literature [1,2]. These models are principally based on several postulates regarding source term modelling methods (shape, source distribution of energy), on the one hand, and effects of the boundary, on the other hand. This paper addresses the problem of the influence of these approximations on the calculated thermal fields within the context of a 2D approach.

The sensitivity of the thermal field to the source size and to the presence of a boundary is successively discussed. The cases of moving line sources and Gaussian cylindrical sources, vibrated or not, are developed. Finally, the effects of boundaries, which have never been studied so far as regards analytical models, are discussed by comparing the solutions achieved within both limited and infinite media.

2. Description of the analytical models

Thermal field calculations are carried out using analytical models with the following characteristics. The 2D diffusive approach of heat transfers using vibrated or non-vibrated sources within limited or infinite regions is examined here. The modelled plane corresponds to an infinite length in the direction of the source (y) and to a width, L, in the transverse direction (x). The speed of the 2D source is v and the temperature far from the source is T_0. The thermophysical properties (conductivity λ, diffusivity a) and the convection coefficient at the boundary h are assumed to be independent from the temperature.

The temperature field in the frame of reference of the source is given by the following quasi-stationary system of equations:

$$\frac{\partial^2 \boldsymbol{T}}{\partial x^2} + \frac{\partial^2 \boldsymbol{T}}{\partial y^2} + \frac{\boldsymbol{v}}{\boldsymbol{a}} \frac{\partial \boldsymbol{T}}{\partial \boldsymbol{y}} + \frac{\boldsymbol{S}(\boldsymbol{x},\boldsymbol{y})}{\lambda} = 0 \quad (1)$$

* Corresponding author. Tel./fax: +3302-97-87-45-52/00.
E-mail addresses: philippe.rogeon@univ-ubs.fr (P. Rogeon), dcn.indret@wanadoo.fr (R. Berthet).
[1] Tel./fax: +3302-40-84-85-59/87-87.

0017-9310/$ - see front matter
doi:10.1016/S0017-9310(03)00288-6

Nomenclature

a	thermal diffusivity (m^2/s)	x,y,z	spatial coordinates (m)
Bi	Biot number	δ_T	amplitude according to the Y-axis (m)
H	source depth (m)	ω	apparent radius of the source (m)
h	transfer coefficient ($W/m^2\,K$)	λ	thermal conductivity (W/m K)
L	sample half-width (m)	δ_L	amplitude according to the X-axis (m)
P	welding power (W)	v	index indicating the vibrated source
$r_{99\%}$	Gaussian source radius (m)	$*$	associated with dimensionless variables in relation to L
$S(x,y)$	volumic source density (W/m^3)		
T_0	temperature far from the source (°C)	$+$	associated with dimensionless variables in relation to ω
$T(x,y)$	temperature field (°C)		
u	Peclet number	i	index indicating the infinite environment
v	welding velocity (m/s)	0	index indicating the moving line source

$$\boldsymbol{x}=0 \quad \frac{\partial \boldsymbol{T}}{\partial \boldsymbol{x}}=0 \tag{2}$$

$$\boldsymbol{x}=\boldsymbol{L}-\lambda\frac{\partial \boldsymbol{T}}{\partial \boldsymbol{x}}=\boldsymbol{hT} \quad \text{or} \quad \boldsymbol{y}\to\pm\infty \quad \boldsymbol{T}=\boldsymbol{T}_0 \tag{3}$$

$$\boldsymbol{y}\to\pm\infty \quad \boldsymbol{T}=\boldsymbol{T}_0 \tag{4}$$

The source is modelled using an axisymmetric volumic source, whose height is H, in the direction perpendicular to the calculation plane (z). The power density volumic distribution is assumed to be uniform in line and Gaussian in the transverse plane (x,y). This Gaussian distribution is parameterized from the radius ω, which is used to control both the peak and the shape of the distribution., which also represents the standard deviation of the regular distribution, is therefore statistically considered as the reference mean radius of the source. Since the Gaussian source becomes identified with a moving line source when the apparent radius, ω, tends towards 0. The vibration of the source is developed using two periodical functions with which the beam describes an ellipse (the amplitudes are δ_L along the X-axis and δ_T along the Y-axis) [3].

The non-vibrated and elliptic vibrated Gaussian sources are, respectively:

$$S(x,y)=\left[\frac{P}{H}\right]\exp\left(-\frac{x^2+y^2}{2\omega^2}\right)\frac{1}{2\pi\omega^2} \tag{5}$$

$$\boldsymbol{S}(\boldsymbol{x},\boldsymbol{y})=\left[\frac{\boldsymbol{P}}{\boldsymbol{H}}\right]\exp\left(-\frac{\boldsymbol{x}^2+\boldsymbol{y}^2}{2\omega^2}\right)\frac{1}{4\pi^2\omega^2}\times\exp\left(-\frac{\delta_T^2}{8\omega^2}\right)\int_0^{2\pi}\exp\left(\left(\frac{\delta_T^2-\delta_L^2}{8\omega^2}\right)\cos^2(\theta)+\frac{\delta_L}{2\omega^2}\boldsymbol{x}\cos(\theta)+\frac{\delta_T}{2\omega^2}\boldsymbol{y}\sin(\theta)\right)\mathrm{d}\theta \tag{6}$$

Table 1 gives the solutions of the dimensionless temperature fields $T^+(x^+,y^+)$. The dimensional solutions of the temperature fields are then deduced (with a reference temperature, T_r, expressed by $P/(2\pi H\lambda)$) from:

$$T(x^+,y^+)=T^+(x^+,y^+)T_r+T_0 \tag{7}$$

3. Impact of the source size on the thermal field

The sensitivity of the source size on the thermal field is examined by comparing the Gaussian and line source solutions within an infinite region, successively. In this case, the following ratios are defined:

$$M_i=\frac{T_{i0}(x^+,y^+)}{T_i(x^+,y^+)}=\frac{T_{i0}^+(x^+,y^+)+T_r^+}{T_i^+(x^+,y^+)+T_r^+} \tag{8}$$

for the non-vibrated source (with T_r^+ expressed by T_0/T_r) and for the vibrated source:

$$V_i=\frac{T_{i0}(x^+,y^+)}{T_{iv}(x^+,y^+)}=\frac{T_{i0}^+(x^+,y^+)+T_r^+}{T_{iv}^+(x^+,y^+)+T_r^+} \tag{9}$$

The variation ranges of the various dimensionless and dimensional physical units have been chosen to cover all the welding configurations available in electron beam welding [4]. These parameter ranges, however, require some adjustments to suit other welding processes. In the considered range, T_r^+ negligible compared to the dimensionless temperature fields, has a limited effect on the calculation of the ratios M_i and V_i. Subsequently, only the highest value, namely 0.4, is considered.

Fig. 1 presents the evolution of the criteria M_i and V_i when y^+ changes from −20 to +10, for x^+ equal to 0, for Peclets' both extremes and for the maximum amplitude ($\delta_T^+=\delta_L^+=10$).

In the case of the non-vibrated Gaussian source, the effect of the source size is felt mainly within the distribution area of the power density. The range of influence is limited to the radius of source $r_{99\%}$, which is defined, for a Gaussian distribution, by (2.8 ω). Within this area, for y^+ ranging between −2.8 and 2.8, the distortion intensity is even more strong since the Peclet number is high. A high Peclet number, indeed, conflicts with the quick diffusion of the energy supplied by the beam.

Table 1
Dimensionless solutions of the temperature field

Dimensionless solutions of the temperature field within limited regions

Non-vibrated Gaussian source

$$T^+(x^+,y^+)\qquad \frac{\sqrt{2\pi}}{4}\mathrm{e}^{-u^+(y^+-u^+)}\sum_{m=1}^{+\infty}\left\{\frac{\cos(\beta_m^+x^+)}{1/2+\frac{\sin(2r\beta_m^+)}{4r\beta_m^+}}\frac{Q_m^+\mathrm{e}^{\beta_m^{+2}/2}}{K_m^+}\begin{pmatrix}\mathrm{e}^{K_m^+(y^+-u^+)}erfc\left(K_m^+/\sqrt{2}+(y^+-u^+)/\sqrt{2}\right)\\+\mathrm{e}^{-K_m^+(y^+-u^+)}erfc\left(K_m^+/\sqrt{2}-(y^+-u^+)/\sqrt{2}\right)\end{pmatrix}\right\}$$

Vibrated Gaussian source

$$T_v^+(x^+,y^+)\qquad \frac{\sqrt{2\pi}}{4}\mathrm{e}^{-u^+(y^+-u^+)}\int_0^{2\pi}\frac{\mathrm{e}^{u^+\delta_T^+\sin(\theta)}}{2\pi}\sum_{m=1}^{+\infty}\left\{\frac{\cos(\beta_m^+x^+)}{1/2+\frac{\sin(2r\beta_m^+)}{4r\beta_m^+}}\frac{Q_v^+\mathrm{e}^{\beta_m^{+2}/2}}{K_m^+}\begin{pmatrix}\mathrm{e}^{K_m^+(y^+-\delta_T^+\sin(\theta)-u^+)}erfc(K_m^+/\sqrt{2}+(y^+-\delta_T^+\sin(\theta)-u^+)/\sqrt{2})\\+\mathrm{e}^{-K_m^+(y^+-\delta_T^+\sin(\theta)-u^+)}erfc(K_m^+/\sqrt{2}-(y^+-\delta_T^+\sin(\theta)-u^+)/\sqrt{2})\end{pmatrix}\right\}\mathrm{d}\theta$$

Non-vibrated line source

$$T_0^+(x^+,y^+)\qquad \pi\mathrm{e}^{-u^+y^+}\sum_{m=1}^{+\infty}\left(\frac{\cos(\beta_m^+x^+)}{r+\frac{\sin(2r\beta_m^+)}{2\beta_m^+}}\right)\frac{\mathrm{e}^{-K_m^+|y^+|}}{K_m^+}$$

Vibrated line source

$$T_{0v}^+(x^+,y^+)\qquad \pi\mathrm{e}^{-u^+y^+}\int_0^{2\pi}\frac{\mathrm{e}^{u^+\delta_T^+\sin(\theta)}}{2\pi}\sum_{m=1}^{+\infty}\left(\frac{\cos(\beta_m^+x^+)}{r+\frac{\sin(2r\beta_m^+)}{2\beta_m^+}}\right)\cos(\beta_m^+\delta_L^+\cos(\theta))\frac{\mathrm{e}^{-K_m^+|y^+-\delta_T^+\sin(\theta)|}}{K_m^+}\mathrm{d}\theta$$

Dimensionless solutions of the temperature field within infinite regions

Non-vibrated Gaussian source

$$T_i^+(x^+,y^+)\qquad \frac{\mathrm{e}^{-u^+(y^+-u^+)}}{2}\int_0^{+\infty}\frac{\cos(\beta^+x^+)}{K^+}\begin{pmatrix}\mathrm{e}^{K^+(y^+-u^+)}erfc\left(K^+/\sqrt{2}+(y^+-u^+)/\sqrt{2}\right)\\+\mathrm{e}^{-K^+(y^+-u^+)}erfc\left(K^+/\sqrt{2}-(y^+-u^+)/\sqrt{2}\right)\end{pmatrix}\mathrm{d}\beta^+$$

Vibrated Gaussian source

$$T_{iv}^+(x^+,y^+)\qquad \frac{\mathrm{e}^{-u^+(y^+-u^+)}}{2}\int_0^{2\pi}\frac{\mathrm{e}^{u^+\delta_T^+\sin(\theta)}}{2\pi}\int_0^{+\infty}\frac{\cos(\beta^+x^+)}{K^+}\cos(\beta^+\delta_L^+\cos(\theta)\begin{pmatrix}\mathrm{e}^{K^+(y^+-\delta_T^+\sin(\theta)-u^+)}erfc(K^+/\sqrt{2}+(y^+-\delta_T^+\sin(\theta)-u^+)/\sqrt{2})\\+\mathrm{e}^{-K^+(y^+-\delta_T^+\sin(\theta)-u^+)}erfc(K^+/\sqrt{2}-(y^+-\delta_T^+\sin(\theta)-u^+)/\sqrt{2})\end{pmatrix}\mathrm{d}\beta^+\,\mathrm{d}\theta$$

Non-vibrated line source

$$T_{i0}^+(x^+,y^+)\qquad \mathrm{e}^{-u^+y^+}K_0\left(u^+\sqrt{x^{+2}+y^{+2}}\right)$$

Vibrated line source

$$T_{i0v}^+(x^+,y^+)\qquad \mathrm{e}^{-u^+y^+}\int_0^{2\pi}\frac{\mathrm{e}^{u^+\delta_T^+\sin(\theta)}}{4\pi}\left(K_0\left(u^+\sqrt{(x^+-\delta_L^+\cos(\theta))^2+(y^+-\delta_T^+\sin(\theta))^2}\right)+K_0\left(u^+\sqrt{(x^+-\delta_L^+\cos(\theta))^2+(y^+-\delta_T^+\sin(\theta))^2}\right)\right)\mathrm{d}\theta$$

Dimensionless values

r	L/ω	y^+	y/ω	Bi^+	$(h\omega)/\lambda$	β_m^+	$r\beta_m^+\tan(r\beta_m^+)=rBi^+$
u^+	$(v\omega)/(2a)$	δ_L^+	$\delta_L/2\omega$	Q_m^+	$\frac{1}{r}\int_0^r\mathrm{e}^{-(x^2/2)}\cos(\beta_m^+x)\,\mathrm{d}x$	Q_v^+	$\frac{\mathrm{e}^{-\frac{\delta_L^{+2}}{2}\cos^2(\theta)}}{r}\int_0^r\mathrm{e}^{-\frac{x^2}{2}+\delta_L^+x\cos(\theta)}\cos(\beta_m^+x)\,\mathrm{d}x$
x^+	x/ω	δ_T^+	$\delta_T/2\omega$	K_m^+	$\sqrt{u^{+2}+\beta_m^{+2}}$	K^+	$\sqrt{u^{+2}+\beta^{+2}}$

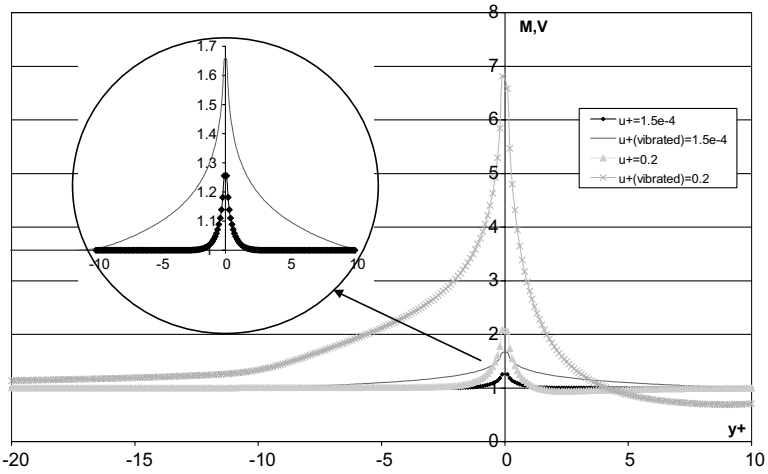

Fig. 1. Evolution of M and V according to y^+.

On the other hand, while a perfect distortion symmetry is established within $r_{99\%}$ for low values of u^+ ($u^+ = 1.5 \times 10^{-4}$), it is not so for high values of u^+ ($u^+ = 0.2$). The thermal pumping effect at the head of the source due to the material flux for high u^+, generates high thermal gradients near the head of the source (Gaussian sources, which are larger, are used for more extensive heating). The criterion M_i is then lower than 1.

When examining the effects of the vibration on the thermal fields in the weld metal zone using conductive transfer analysis methods, in which convective transfers are ignored, we obtain conclusions similar to those of the previous paragraph. In pure conduction conditions, the effect of the source size due to the vibration, in comparison with an identical non-vibrated source, is felt exclusively within the vibration area.

As regards electron beam welding, beam vibrations are principally used to avoid instability problems by affecting the thermohydraulic features of the welded metal. Vibration shapes and frequencies of the electron beam are adjusted empirically to optimize weld beads. The source vibration is equivalent to the extension of the source size and, therefore, to the reduction of the power density in the supply zone.

It has been shown here that the effect of the source size is limited to the radius, within which the power density is supplied. The simpler solutions of the moving line source within infinite regions may, therefore, be preferred when areas beyond the radius $r_{99\%}$ are examined (welded or heat affected zones of a metal, for instance). Moreover, it is important to notice that reducing the problem to moving line sources makes it possible to free oneself from the problem of defining both source size and power distribution (Gaussian, uniform, etc.).

4. Boundary effect

In order to analyze the influence of the boundary on the solution, the thermal field, $T(x^+, y^+)$, calculated in the half-plane of width L is compared with the thermal field, $T_i(x^+, y^+)$, in the half-plane of infinite width. The factor G is defined as the ratio of the temperature fields $T_i(x^+, y^+)$ and $T(x^+, y^+)$. The solutions using line sources within regions of finite and infinite width are used to calculate G:

$$G = \frac{\boldsymbol{T}_i(\boldsymbol{x}, \boldsymbol{y})}{\boldsymbol{T}(\boldsymbol{x}, \boldsymbol{y})} = \frac{\boldsymbol{T}_i^+(\boldsymbol{x}^+, \boldsymbol{y}^+) + \boldsymbol{T}_r^+}{\boldsymbol{T}^+(\boldsymbol{x}^+, \boldsymbol{y}^+) + \boldsymbol{T}_r^+} \tag{10}$$

For a better understanding of the results, the solutions are associated with new dimensionless variables (noticed with $*$) based on the half-width of the sample L ($vL/2a$) is the Peclet number, (x/L) and (y/L) the coordinates).

The Biot number, Bi, is associated to the boundary ($x^* = 1$). The effect of the boundary on the thermal field is twofold: through the variable u^*, which expresses the lack of metal, the boundary tends to generate an overheating of the piece and brings values of G lower than 1. However, with the associated Biot number, the effect is opposite and may bring values of G higher than 1.

The evolutions of G are studied for the following dimensionless parameter values: coordinates $x^* = 0.1$ and $y^* = 0.1$; power temperature $T_r^+ = 0.4$; dimensionless velocity u^* from 0.05 to 10; Biot number from 0.0001 to 1. The present study is limited here to the influence of u^* and Bi on G whereas the conclusions are based on works developed in reference [4].

For the highest Peclet number of u^* within the range 1–10, the evolution of G remains below 10% whatever the Biot number. On the other hand, for the lowest Peclet number of u^* within the range 0.05–1, G presents

a sharp evolution on the order of 80% and the boundary effect cannot be neglected anymore. The conflicting effects of u^* and Bi on G are particularly noticeable.

Low Biot ranges (from 0.0001 to 0.01): the effect of u^* is most dominant and G decreases from 0.9 to 0.2 when u^* decreases from 1 to 0.05. When u^* is 0.05, however, a Biot compensation phenomenon is observed, which tends to oppose the decrease of G. High Biot ranges (from 0.01 to 1): for a Biot number equal to 0.01, the effect of u^* is most dominant. For Bi higher than 0.01 and Peclet numbers within the range 1–0.5, the Biot number effect becomes most dominant when the Peclet number get lower (G becomes higher than 1).

5. Application to electron beam welding

The analytical or numerical calculation of heat transfers within metal parts using electron beam welding (EBW) is traditionally based on Gaussian-type source modelling. This type of source model is no more than a simplistic representation of the complexity of the phenomenon of energy deposition on the keyhole walls during EBW. However, for the determination of the microstructural transformations within the weld bead, the thermal fields are calculated in areas far enough from the centre of the source (heat affected zone, weld metal zone). Moreover, before welding metal massive workpieces and in order to adjust welding parameters, welders usually carry out welding tests on samples with same thickness but smaller width. Depending on the material and with similar welding parameters, welding beads generated in the sample or in the massive workpiece can be different. When the sample width, indeed, is too small, overheat problems may appear and the welding bead widens. The model presented here makes it possible to estimate weld bead widening critical conditions.

The model described in the first section fits deep welding processes (electron and laser beams) under both following welding conditions: full penetration (general case) or partial penetration with optimum focusing. The energy distribution is considered to be uniform along the depth and generates a weld bead, whose width is uniform on the greater part of its height, save for the beam input and output zones in the case of full penetration welds, and near the bead head and root in the case of welds in partial penetration mode. Under these conditions, the temperature field within the metal can be assumed to be two-dimensional in the cross-section, z.

The very high energy density found in the beam creates a thin and deep keyhole, on the walls of which the energy is supplied. The vapour capillary is modelled using an axisymmetric source, whose height, H, is equal to that of the keyhole. This height is identical to the piece thickness in full penetration welding mode and to the penetration depth in partial penetration welding mode. The power energy volumic distribution is assumed to be uniform in the depth, and Gaussian transversely. Specific welding tests carried out on stainless steel, tungsten and carbon strips according to Arata's method [6] are used to determine the shape of the beam and to calibrate the standard deviation, ω, of the Gaussian distribution from the beam diameter in the focal plane.

The EBW machine of the DCN Indret is used here to make horizontal test butt welds on samples equipped with temperature sensors [5]. The tests are carried out on 18MND5 steel samples. The embedding method chosen for the temperature sensors consists in (Fig. 2): the cutting into transverse slices of the sample; the fine instrumentation, with temperature sensors, of the first polished interfaces; the re-soldering and clipping using TIG (tungstene inert gas) welding.

The welding test conditions are: welding parameters ($P = 17.4$ kW, $v = 2.5$ mm/s, $\omega = 0.355$ mm); thermophysical properties of steel ($\lambda = 32$ W m/K, $a = 6.25$ mm^2/s); radiative heat transfer condition at the limit ($h = 10$ W/m^2 K); sample size ($L = 50$ mm, $H = 75$ mm); thermocouple position ($x = 2.54$ mm, $x = 8$ mm).

Despite the approximations consented at the level of the analytical model (properties independent of the temperature, neglected latent heat, convection neglected in the welded metal, etc.), a goodness of fit of the theoretical and experimental thermal cycles is observed (Fig. 3). This satisfactory comparison between the results of the analytical model and the experimental recording demonstrate that, provided that the studied areas are located sufficiently far from the energy deposit zone, the predictive results for the thermal fields, achieved using the proposed analytical model, are reasonably accurate.

6. Conclusions

The specific analytical models, developed to compute thermal fields within materials subjected to moving heat sources, find immediate application in welding processes. 2D analytical solutions using vibrated/non-vibrated Gaussian cylindrical or line source models are proposed here. These solutions are applied to an infinite longitudinal half-plane and to a limited width semi-infinite longitudinal half-plane. The sensitivity of the thermal fields to both the source size and the boundary is studied.

The validation is conducted by comparing the solutions with the classical analytical solution of the moving line source in infinite plane, on the one hand, and with experimental thermal cycles recorded from a sample prepared at the DCN Indret using electron beam welding techniques.

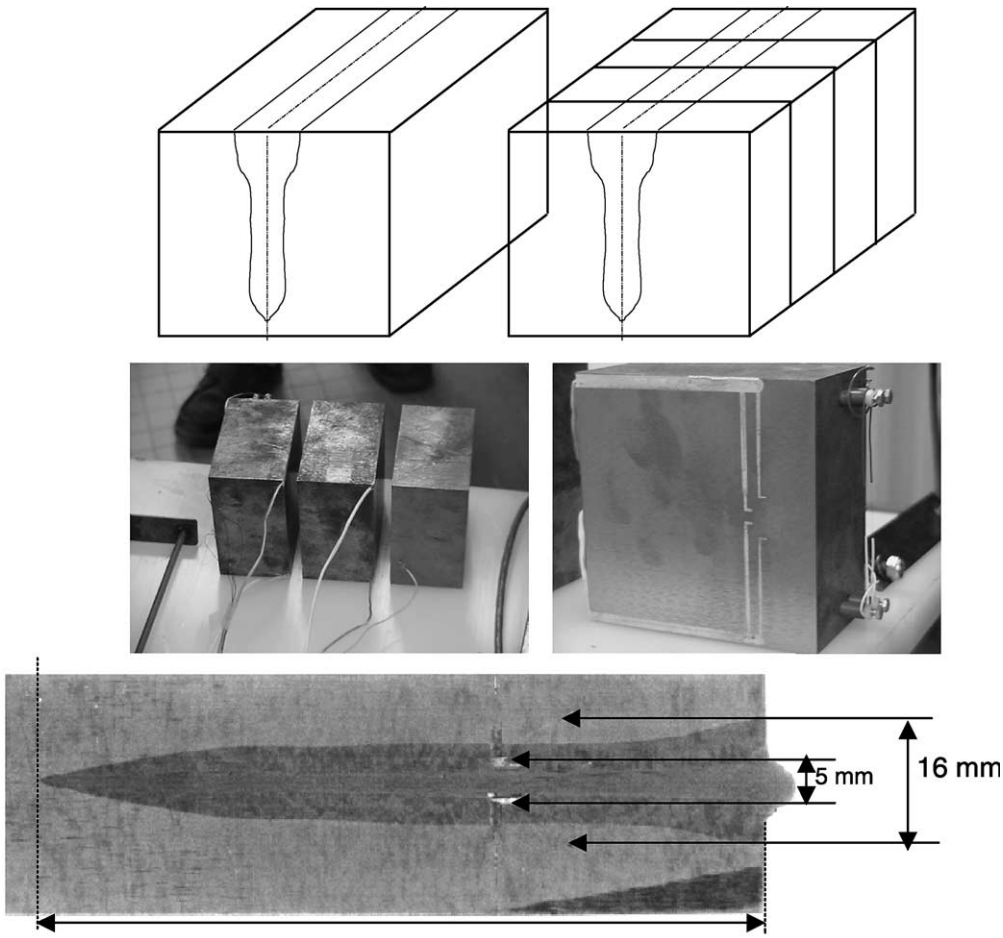

Fig. 2. Sample equipment and sensor embedding at the interfaces.

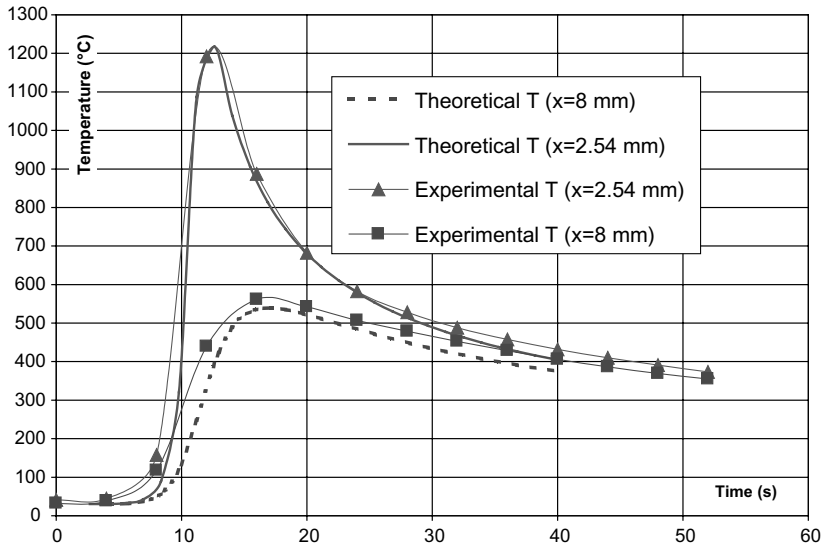

Fig. 3. Comparison between experimental and theoretical cycles of 18MND5 steel.

The impact of the source size on the thermal fields is examined by comparing vibrated and non-vibrated Gaussian sources with a moving line source. This impact proves negligible from the moment that the energy input zone is not considered. In this zone, indeed, the distortion is all the smallest since the effect of the influencing parameters is directed towards an increase of the thermal diffusivity (low Peclet number or vibrated source).

The impact of the boundary (low width welding sample) on the thermal fields shows itself in two antagonistic ways. The material deficiency can generate an overheat of the metal part, whereas, conversely, boundary heat transfers tend to increase the cooling of the part. The results show that the impact of the boundary is negligible for high Peclet numbers and very strong, on the other hand, for low Peclets. High Biot number values, then, contribute to soften the Peclet number effect and even to reverse it.

The 2D analytical models presented in this study demonstrate the usefulness and reliability of the analytical approach, which is too often neglected for more complex numerical approaches. These models are complementary of already available models and fit the requirements of the specific conditions met, for instance, with welding processes better.

References

[1] M.J. Bibby, J.A. Goldak, G.Y. Shing, A model for predicting the fusion and heat affected zone sizes of deep penetration welds, Can. Metall. Quart. 24 (1) (1985) 101–105.

[2] N.T. Nguyen, A. Ohta, Analytical solutions for transient temperature of semi-infinite body subject to 3D moving heat sources, Welding Research Supplement AWS, August 1999, pp. 265–274.

[3] M. Costantini, Simulation numérique du soudage par faisceau d' électrons. Contribution au développement d'un modèle prédictif de l'apport d'énergie, Phd thesis, Université Paris 6, 1985.

[4] P. Rogeon, D. Couëdel, D. Carron, P. Lemasson, J.J. Quemener, Determination of critical sample width for electron beam welding process using analytical model, Heat Transfer Eng. 24 (5) (2003).

[5] P. Rogeon, D. Couedel, D. Carron, P. Lemasson, J.J. Quemener, Numerical simulation of electron beam welding of metals: Sensitivity study of a predictive model, 5th International Seminar on numerical Analysis of Weldability—October 99 Graz-Seggau (Austria) Mathematical Modelling of Weld Phenomena 5, pp. 913–943.

[6] Y. Arata, Evaluation of beam characteristics, in: Y. Arata (Ed.), Plasma, Electron and Laser Beam Technology, ASME, New York, 1986.